VIROLOGY 245, 33–46 (1998)
ARTICLE NO. VY989146

Internal\Structures Containing Transcriptase-Related Proteins in Top Component Particles of Mammalian Orthoreovirus

Kelly A. Dryden,*,‡[1,2] Diane L. Farsetta,§[1] Guoji Wang,*,[3] Jesse M. Keegan,‡,[4] Bernard N. Fields,†,‡ Timothy S. Baker,* and Max L. Nibert‡,[5]

*Department of Biological Sciences, Purdue University, West Lafayette, Indiana 47907; ‡Department of Microbiology and Molecular Genetics and Shipley Institute of Medicine, Harvard Medical School, Boston, Massachusetts 02115; and §Department of Biochemistry, Institute for Molecular Virology, and Cellular and Molecular Biology Program, University of Wisconsin-Madison, Madison, Wisconsin 53706

Received January 20, 1998; accepted March 12, 1998

The structure of mammalian orthoreovirus top component particles, which are profoundly deficient in the content of double-stranded RNA genome, was determined at 30 Å resolution by transmission cryoelectron microscopy and three-dimensional image reconstruction. Previously undetected, ordered densities, appearing primarily as pentameric flowers in the reconstruction, were seen to extend 65 Å inwardly from the inner capsid at the icosahedral fivefold axes. Identically positioned but lower density elements were observed in two types of partially uncoated top component particles obtained by limited proteolysis. The levels of three inner-capsid proteins—λ1, λ3, and μ2—were reduced in concert with the internal densities during proteolytic uncoating. Since λ3 contains the catalytic regions of the viral RNA polymerase and since both λ1 and μ2 appear to play roles in transcription or mRNA capping, the internal structures are concluded to be complexes of the viral transcriptase-related enzymes. The findings have implications for the mechanisms of transcription and mRNA capping by orthoreovirus particles.

INTRODUCTION

Virions of mammalian orthoreoviruses (diameter ≈ 850 Å) contain two icosahedral capsids: a $T = 13$(levo) outer capsid comprising proteins λ2, μ1/μ1C, σ1, and σ3 and a putatively $T = 1$ inner capsid comprising proteins λ1, λ3, μ2, and σ2. Limited proteolysis of virions is commonly used to produce two types of subvirion particles—infectious subvirion particles (ISVPs) and cores—which exhibit distinct differences in their outer capsids. Since cores can produce capped mRNAs in an *in vitro* reaction (Skehel and Joklik, 1969; Banerjee and Shatkin, 1970; Shatkin, 1974; Furuichi *et al.,* 1975), the proteins that they retain—λ1, λ2, λ3, μ2, and σ2—must include all the transcription and capping enzymes. For further discussion of orthoreovirus structure see Dryden *et al.* (1993).

To synthesize the viral mRNAs, cores mediate a series of enzymatic reactions (Furuichi *et al.,* 1975), some of which have been ascribed to specific proteins. The λ3 protein contains the catalytic regions of the RNA polymerase (Koonin, 1992; Starnes and Joklik, 1993). Proteins μ2 (Yin *et al.,* 1996) and λ1 (Morgan and Kingsbury, 1981; Powell *et al.,* 1984) play apparent roles in transcription as well, perhaps through interactions with λ3 (Starnes *et al.,* 1993; Sherry and Blum, 1994; Haller *et al.,* 1995). Proteins μ2 (Noble and Nibert, 1997) and λ1 (Noble and Nibert, 1997; Bisaillon *et al.,* 1997) also influence one or more NTPase activities in cores, which may represent the capping RNA triphosphatase (Noble and Nibert, 1997; Bisaillon and Lemay, 1997) and RNA helicase (Rankin *et al.,* 1989; Noble and Nibert, 1997; Bisaillon *et al.,* 1997), and/or some other NTP-dependent enzyme for RNA metabolism. The λ2 protein constitutes the capping guanylyltransferase (Cleveland *et al.,* 1986; Fausnaugh and Shatkin, 1990; Mao and Joklik, 1991) and may also mediate one or both of the capping methyltransferase activities (Seliger *et al.,* 1987; Koonin, 1993). The σ2 protein is not directly linked to any enzymatic activities, but is needed along with λ1 to form the core shell (Xu *et al.,* 1993).

The orthoreovirus genome comprises 10 segments of double-stranded (ds)RNA, which are templates for transcription. Transcription is asymmetric and conservative, yielding full-length plus-sense RNAs that are released from cores, while the genomic dsRNAs remain particle-bound (Skehel and Joklik, 1969; Banerjee and Shatkin, 1970; Levin *et al.,* 1970). Electron micrographs of transcribing cores show multiple RNAs exiting single particles (Bartlett *et al.,* 1974), suggesting that multiple tran-

† Deceased.

[1] These authors made equivalent contributions.

[2] Present address: School of Biological Sciences, University of Auckland, Auckland, New Zealand.

[3] Present address: Department of Pathology, University of Pittsburgh School of Medicine, Pittsburgh, PA 15261.

[4] Present address: Genzyme Corporation, Framingham, MA 01701.

[5] To whom correspondence and reprint requests should be addressed at Institute for Molecular Virology, University of Wisconsin-Madison, 1525 Linden Drive, Madison, WI 53706. Fax: (608) 262-7414. E-mail: mlnibert@facstaff.wisc.edu.

0042-6822/98 $25.00

scriptases simultaneously transcribe mRNAs from different genome segments. Evidence that the transcriptases are fixed near the fivefold axes include (1) the RNA polymerase λ3 is found in ~12 copies per core, or one per fivefold axis; (2) pentamers of the guanylyltransferase λ2 form turret-like structures that protrude around each fivefold axis (White and Zweerink, 1976), in good position to act on mRNAs extruded from nearby sites (Bartlett *et al.,* 1974; Yeager *et al.,* 1996); and (3) the λ2 and λ3 proteins can interact in solution (Starnes and Joklik, 1993). In response to such findings, other investigators (Joklik, 1983; Shatkin and Kozak, 1983) proposed the moving-template model of orthoreovirus transcription, in which a viral polymerase is fixed at the base of each λ2 pentamer. Although this model is widely accepted in the field, visualization of transcriptase complexes in orthoreovirus particles has not been reported to date.

Previous studies of mammalian orthoreovirus virions, ISVPs, and cores using cryo-TEM and 3-D reconstruction permitted many viral proteins to be assigned to structural features in the capsids (Metcalf *et al.,* 1991; Dryden *et al.,* 1993). However, features attributable to the polymerase protein λ3 and its putative cofactor μ2 were not identified, perhaps because structures at lower radii were obscured by the genomic dsRNA. We were thus interested to determine whether orthoreovirus top component (TC) particles might offer a better view of more internal structures. TC particles (henceforth designated TC virions to distinguish them from derived particle forms) are produced concurrently with virions during infection (Joklik, 1983) but are profoundly deficient in the content of genomic RNA (Smith *et al.,* 1969). Despite the latter, their protein capsids appear very similar to virions upon negative staining and are thought to contain proteins in the same, or similar, amounts as virions (Smith *et al.,* 1969). In the current study we applied cryo-TEM and 3-D image reconstruction to mammalian orthoreovirus TC virions in an effort to visualize structures attributable to the viral transcriptase complexes.

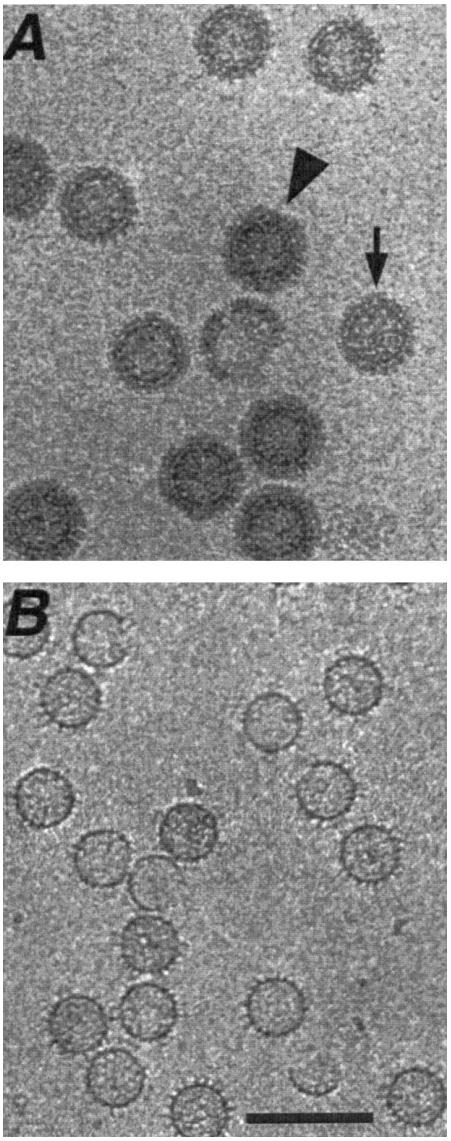

FIG. 1. Cryoelectron micrographs of orthoreovirus TC particles. Purified TC virions and TC ISVPs (A) or TC cores (B) of orthoreovirus T1L were frozen in vitreous ice and imaged with low-dose cryo-TEM procedures. A virion (arrowhead) and ISVP (arrow) are identified in (A). Bar, 100 nm.

RESULTS

Cryo-TEM and 3-D image reconstruction of TC virions

Cryoelectron micrographs of orthoreovirus type 1 Lang (T1L) virions revealed spheroidal particles with a diameter of 850 Å and a bristly perimeter (Fig. 1A, arrowhead) attributable to protein σ3 (Dryden *et al.,* 1993). The TC virions appeared similar to virions (data not shown), but more hollow, reflecting that they are profoundly deficient in genomic dsRNA (Smith *et al.,* 1969; Harvey *et al.,* 1981). Obviously broken or deformed particles were seen at a similarly low frequency with TC virions (Fig. 1A) as with virions (data not shown), suggesting that most TC virions in our preparations had an intact structure that might be viewed at higher resolution after image processing.

Cryoelectron micrographs of TC virions were used to generate a 3-D reconstruction employing model-based methods (Baker and Cheng, 1996; Fuller *et al.,* 1996). The final reconstruction of TC virions was calculated to a resolution of 30 Å. The surface features of TC virions in the reconstruction (Fig. 2A) appear identical to those of virions. The similarities are especially evident, with the surfaces of TC virions and virions juxtaposed in a composite image (Fig. 3A). Features attributable to outer-capsid proteins σ3, μ1, and λ2 are all discernible in TC virions and show few if any differences from virions (Dryden *et al.,* 1993). Most features of the inner capsid, as viewed in cross sections (Figs. 2B and 3A), also appear identical in TC virions and virions; however, a

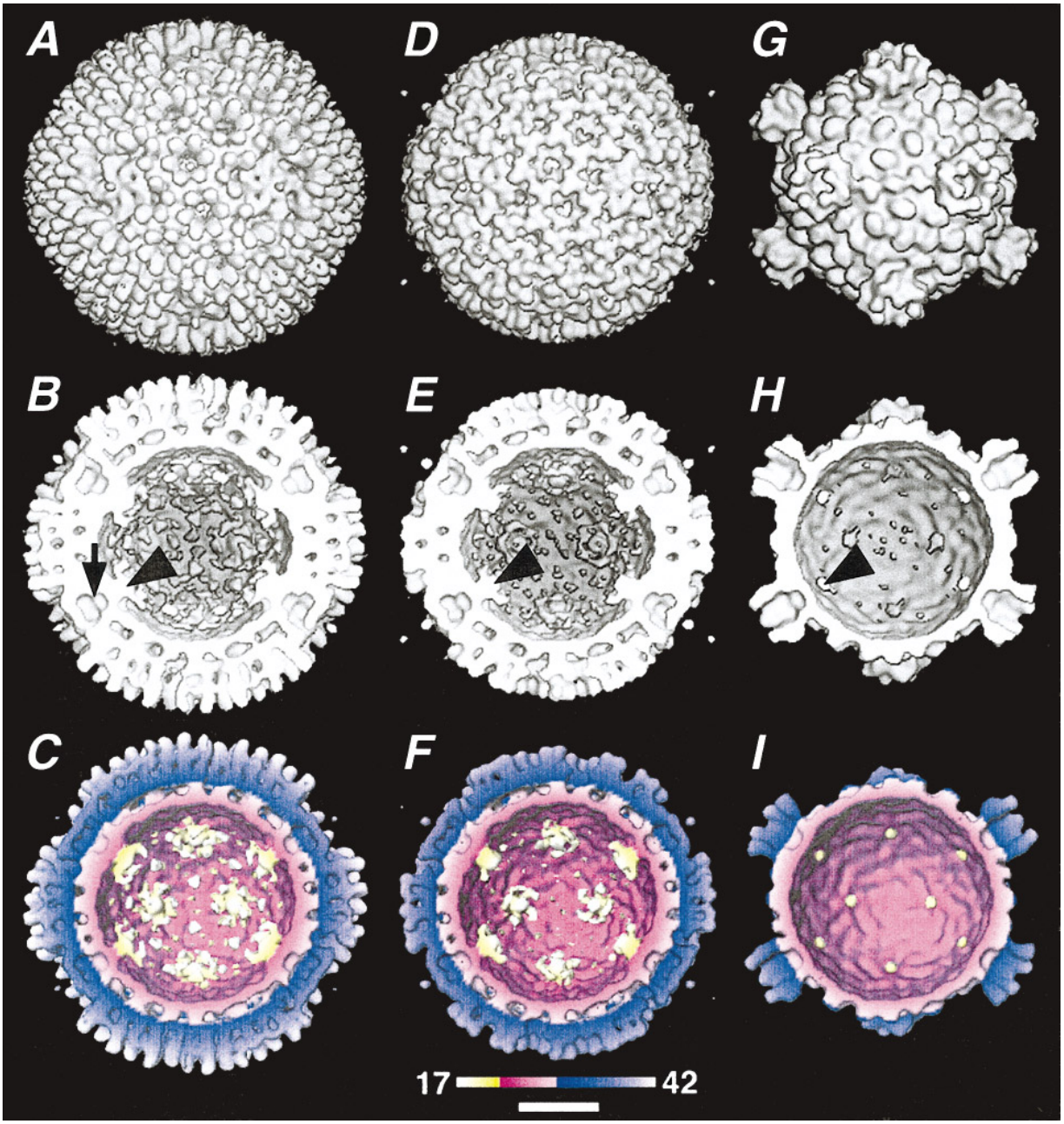

FIG. 2. 3-D image reconstructions of orthoreovirus TC particles. 3-D image reconstructions for TC virions (A–C), TC ISVPs (D–F), and TC cores (G–I) of orthoreovirus strain T1L are shown. (A), (D), and (G) are surface-shaded views from a perspective outside each particle. (B, C), (E, F), and (H, I) are cross-sectional views obtained by cutting each particle through a global twofold axis of symmetry and then removing the front half of the particle to reveal internal features. White features in (B), (E), and (H) show where the viral capsids were cut in generating the cross section. The arrowheads in (B), (E), and (H) identify one of the structures that projects inward along the fivefold axes in TC particles and is tentatively ascribed to be the orthoreovirus transcriptase complex. The arrow in (B) identifies the heart-shaped cavity within the outer capsid that is surrounded by the λ2 protein. Color in (C), (F), and (I) was added as a function of radial depth in the particles (Spencer *et al.,* 1997) as indicated in the associated color legend. Shifts in hue were incorporated to designate the major layers in orthoreovirus particles: blue, outer capsid; lavender, core shell; yellow, internal to the core shell. Images in (A, B), (D, E), and (G, H) were generated at a density contour of approximately −9 (see Table 1). Color images in (C), (F), and (I) were generated at a density contour of approximately −13 (see Table 1), to simplify views of the fivefold-related internal structures. Bar, 20 nm.

striking difference is evident at lower radii in that virions are filled with density attributed to the dsRNA genome (Fig. 3A, asterisk), whereas TC virions are more hollow, reflecting that the genome is mostly absent. In addition, the reconstruction of TC virions reveals several types of internal densities, including flower-like structures that project inwardly from the inner capsid along the fivefold axes (Fig. 2B, arrowhead). Other, less well ordered densities are concentrated just beneath the inner capsid around each icosahedral threefold axis (Fig. 2B).

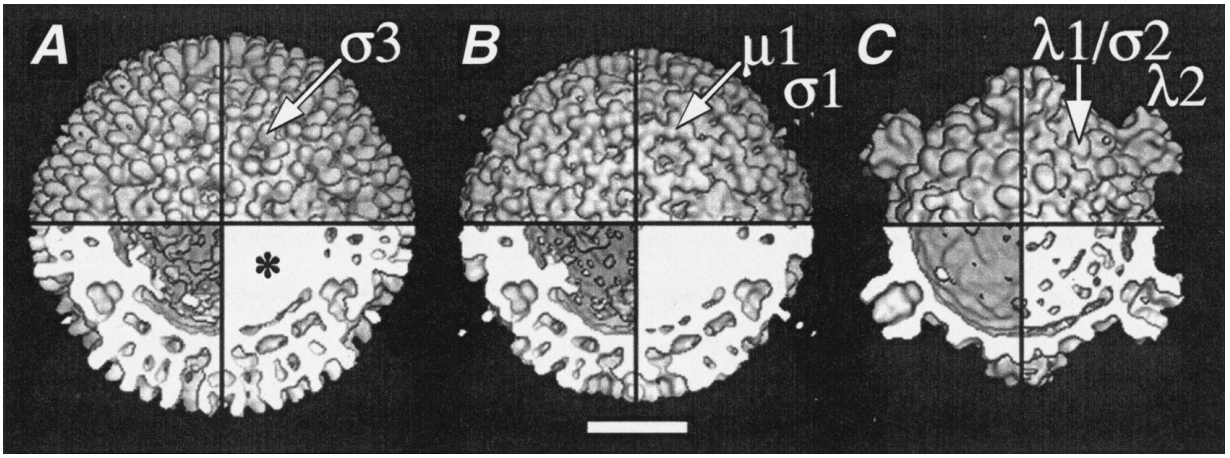

FIG. 3. Composite images of 3-D image reconstructions of orthoreovirus particles. Portions of the 3-D image reconstructions for two types of orthoreovirus T1L particles are combined in each composite: (A) TC virions (left half) and virions (right half); (B) TC ISVPs (left half) and ISVPs (right half); and (C) TC cores (left half) and cores (right half). The top half of each composite includes surface-shaded views from a perspective outside the particles, whereas the bottom half includes cross-sectional views like those in Fig. 2. Reconstructions for virions, ISVPs, and cores are from Dryden *et al.* (1993). The *asterisk* in (A) identifies density in the particle interior that is attributed to the genomic dsRNA and is missing from TC particles. Features attributed to each outer-capsid protein are also labeled in the surface views of these particles (top right quadrants). The μ1 label refers to cleavage products of that protein that are present in virions (μ1N and μ1C; Nibert *et al.,* 1991) and ISVPs (μ1N, μ1δ/δ, and ϕ; Nibert and Fields, 1992). Only the base of the flexible σ1 fiber, which extends $>$400 Å from the particle surface (Furlong *et al.,* 1988), is visible in the virion and ISVP reconstructions. Bar, 20 nm.

Each of the flower-like structures in TC virions is found immediately beneath a cavity within the outer capsid that appears heart-shaped in cross section (Figs. 2B, arrow, and 3A) and is surrounded by subunits of the λ2 pentamer (Dryden *et al.,* 1993). In closer views (Figs. 4A–4F), the structures are seen to have a stalk that is 45 Å in diameter and extends 65 Å into the central cavity of TC virions. The interior end of the stalk is decorated by five "petals" of weaker density, which attach near the stalk's tip and are aligned with capsid ridges that surround its base (Figs. 4C, 4D, and 4F). These ridges, as well as five intervening grooves in the capsid, are best seen when the density contour is increased to remove the lower density petals from obscuring the capsid (Fig. 4D) or when the capsid is viewed at an acute angle at high magnification (Fig. 4F). The locations of the flower-like structures correspond to those proposed for the orthoreovirus transcriptase components (see Introduction).

Cryo-TEM and 3-D image reconstruction of TC ISVPs and TC cores

To address which protein components might constitute the internal densities in TC virions, we generated subvirion particles—TC ISVPs and TC cores—by chymotrypsin treatment of TC virions for image reconstruction. This approach seemed promising since one inner-capsid protein, λ1, was known to undergo cleavage upon chymotrypsin treatment of TC virions (Smith *et al.,* 1969; White and Zweerink, 1976). We hypothesized that the loss of protein mass to protease degradation might be correlated with the loss of internal densities from TC subvirion particles.

Both TC ISVPs (Fig. 1A, arrow) and TC cores (Fig. 1B) were found to resemble the respective genome-containing particles except for a hollow appearance from lower density in their centers. TC ISVPs were 790 Å in diameter and exhibited coarse features on their surfaces attributable to outer-capsid protein μ1 (Dryden *et al.,* 1993). In addition, long fibers representing the cell-attachment protein σ1 (Furlong *et al.,* 1988) were seen extending radially up to 400 Å from the surfaces of some ISVPs. TC ISVPs were easily distinguished from TC virions when mixed on the same grid (Fig. 1A). In TC cores, the exposed inner capsid was 600 Å in diameter, with large features attributable to protein λ2 extending an additional 100 Å around the fivefold axes (White and Zweerink, 1976; Dryden *et al.,* 1993).

3-D reconstructions of TC ISVPs and TC cores, calculated to 30 Å resolution, were generated from micrographs using methods similar to those used with TC virions. In the reconstructions, the outer surfaces of TC ISVPs (Figs. 2D and 3B) and TC cores (Figs. 2G and 3C) appear very similar to those of ISVPs (Fig. 3B) and cores (Fig. 3C). Features attributable to outer-capsid proteins λ2, μ1, and σ1 are all discernible in TC ISVPs and show few differences from ISVPs (Dryden *et al.,* 1993). The 12 turrets that project around the fivefold axes and are attributable to protein λ2 are very similar in TC cores and cores, as are the 150 ellipsoidal nodules that decorate the surfaces of TC cores and cores, and are attributable to inner-capsid proteins λ1 and/or σ2 (Dryden *et al.,* 1993).

As with TC virions, the 3-D reconstructions of TC ISVPs reveal inwardly projecting, flower-like structures at each fivefold axis; however, the densities of these structures

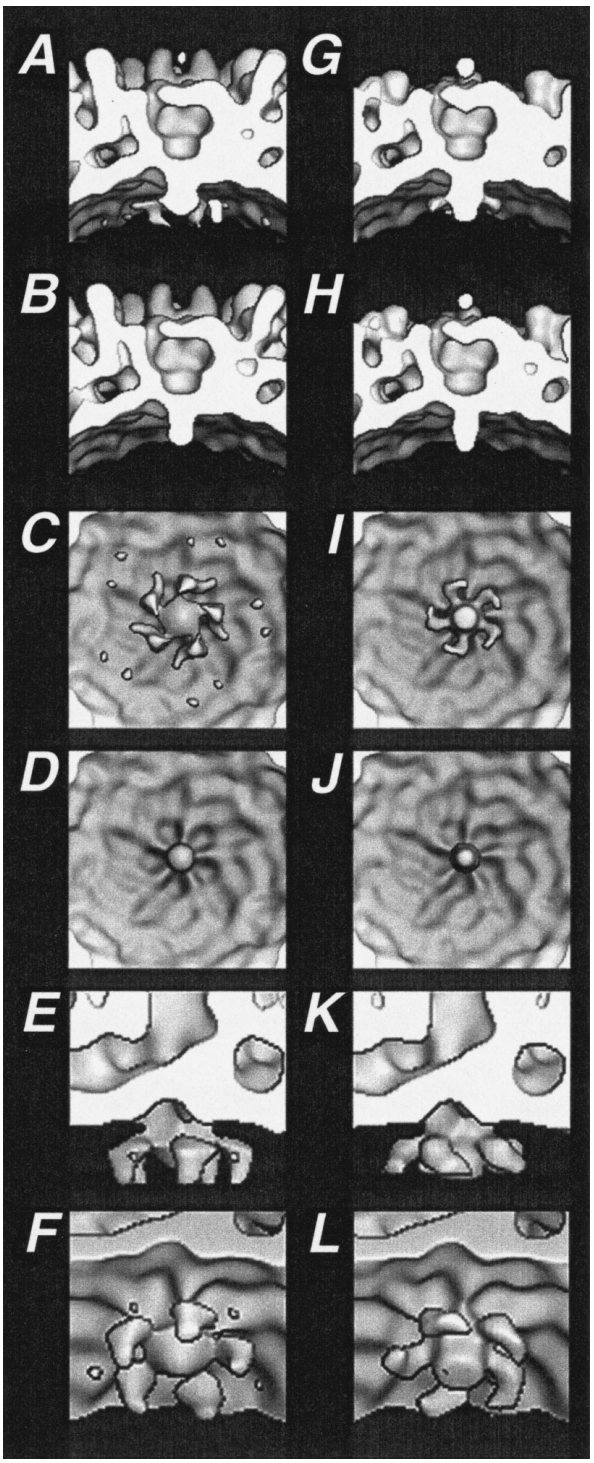

FIG. 4. Magnified views of putative transcriptase complexes in TC virions and TC ISVPs. Views of an internal fivefold structure, tentatively ascribed to be the orthoreovirus transcriptase complex, are shown from TC virions (A–F) and TC ISVPs (G–L). Three types of visualization are included: cross sections through the fivefold region as generated by cutting through each particle along a global twofold axis and then removing the front half of the particle to reveal internal features (A, B, G, H); surface-shaded views of each particle's inner capsid from a perspective inside the particle's central cavity, sighting along a fivefold axis (C, D, I, J); and surface-shaded views of each fivefold structure obtained by cutting through the particle near to, but not on, the global twofold axis so that the structure itself was not sectioned (E, F, K, L). Images in (B), (D), (H), and (J) were generated at a density contour of approximately −20 (see Table 1) to enhance views of the inner-capsid topography. Other images were generated at a density contour of −13 to −14 (see Table 1).

appear somewhat reduced in TC ISVPs (Figs. 2E, arrowhead, and 3B). In addition, the stalk of each structure is slightly longer and narrower than that in TC virions, extending 70 Å from the wall of the inner capsid and having a diameter of 40 Å (Figs. 4G–4L). The five petals are also different in that the points at which they attach to the stalk align with grooves in the capsid (Figs. 4I, 4J, and 4L), rather than with ridges as in TC virions (Figs. 4C, 4D, and 4F). With TC cores, the decrease in density of the flower-like structures is more pronounced. In fact, the structure in TC cores has been reduced to a small spheroidal feature, 25 Å in diameter and disconnected from the inner capsid by 15 Å (Figs. 2H, arrowhead, and 3C). The less well ordered densities beneath the icosahedral threefold axes of the inner capsid are also reduced in both TC ISVPs and TC cores.

Reduced amounts of intact λ1 protein in TC subvirion particles

Inner-capsid protein λ1 (137 kDa)—which is present in 120 copies per reovirion and is a major component of the core shell (Xu *et al.,* 1993)—is cleaved to yield two particle-bound fragments, A (~110K) and B (~100K), when TC virions of orthoreovirus type 3 Dearing (T3D) are treated with chymotrypsin to yield TC cores (Smith *et al.,* 1969; White and Zweerink, 1976). Since both fragments are more than half the size of intact λ1, they must represent overlapping regions of this protein (Smith *et al.,* 1969). Smaller fragments representing parts of λ1 outside A and B are not found, suggesting that they are degraded. In contrast to these findings with λ1, the other major protein in the core shell—σ2—and the core turret protein—λ2—remain uncleaved in TC cores (Smith *et al.,* 1969; White and Zweerink, 1976).

Considering these previous findings, we hypothesized that the part of λ1 lost during chymotrypsin digestion may specifically contribute to internal densities in TC virions. Phosphate–urea–SDS gels provide separation of λ1 from the similarly sized λ2 and λ3 proteins (Cleveland *et al.,* 1986) and were used to analyze λ1 in this study. In initial experiments with orthoreovirus T1L TC virions, timed treatments with chymotrypsin showed that the λ1A and B fragments arose when either TC ISVPs or TC cores were produced (data not shown). In addition, λ1A was shown to arise early but to decrease to low levels as λ1B accumulated toward steady-state levels by 10 min of treatment. These findings suggest that λ1B is derived from λ1A by one or more additional cleavage; moreover, results from quantitative analysis of gels (data not

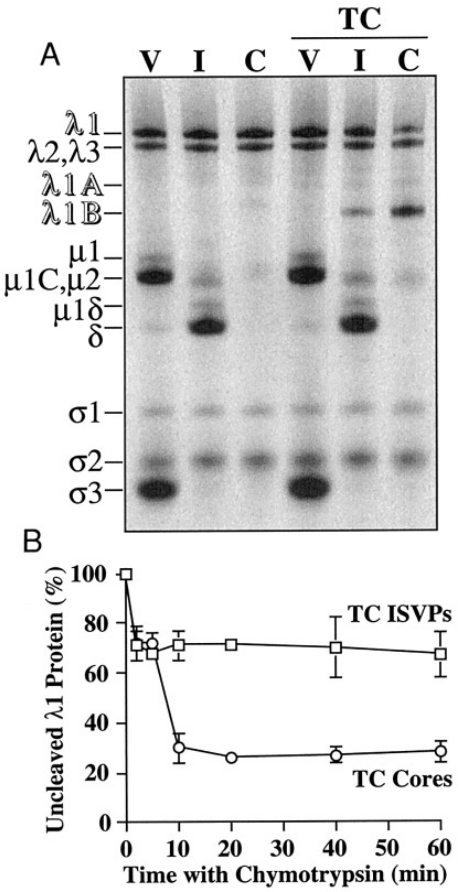

FIG. 5. Status of λ1 protein in orthoreovirus particles. (A) Status of the λ1 protein in six types of orthoreovirus particles—virions (V), ISVPs (I), cores (C), TC virions (TC-V), TC ISVPs (TC-I), and TC cores (TC-C)—was determined by SDS–PAGE and phosphor imaging. Samples containing 6×10^{10} [^{35}S]methionine/cysteine-labeled viral particles were run in each gel lane. This gel was one used for quantitations of λ1 shown in Fig. 6. Positions of orthoreovirus proteins are indicated. (B) Status of λ1 protein at different times during chymotrypsin treatments yielding either TC ISVPs (□) or TC cores (○). Timed treatments were ended by addition of phenylmethylsulfonyl fluoride and cooling to 4°C. Samples containing equal numbers of particles in each treatment series were analyzed by SDS–PAGE, and the intensities of orthoreovirus proteins were quantitated by phosphor imaging.

shown) confirmed that λ1B is relatively resistant to further degradation. Another finding from early experiments was that more λ1 protein was cleaved, and more λ1 B fragment was present at the final steady-state levels, in TC cores than TC ISVPs (see Figs. 5 and 7).

To quantify λ1 levels in different particles, we used ^{35}S-labeled virions, TC virions, and chymotrypsin digests containing subvirion particles of each. Proteins were detected by phosphor imaging. A representative gel (Fig. 5A) shows the reduced levels of λ1 in TC subvirion particles. For comparisons between lanes, the amount of intact λ1 was standardized to the λ2/λ3 band, which is composed mostly of λ2, a protein whose levels were constant in all particles (see Fig. 7; Smith *et al.,* 1969; White and Zweerink, 1976). Results indicated that although the levels of intact λ1 in subvirion particles were 100% of that in virions (103 ± 3% in ISVPs, 107 ± 4% in cores), its levels were reduced in TC subvirion particles relative to TC virions (83 ± 2% in TC ISVPs, 34 ± 2% in TC cores) (Fig. 6). Similar results were obtained with other plaque-derived clones of orthoreovirus T1L, indicating that these are consistent properties of the T1L TC particles prepared by us. In addition, analysis of λ1 levels over times of treatments yielding either TC ISVPs or TC cores as stable products revealed that these approximate levels of intact λ1 are distinct and characteristic of each particle type (Fig. 5B).

Accumulation of a C-terminal Fragment of λ1 in TC subvirion particles

To determine which portion of λ1 is lost from TC subvirion particles, we subjected the λ1B fragment from TC cores to N-terminal sequencing. Because the L3 sequence of orthoreovirus T1L has not been reported, we performed this experiment with orthoreovirus T3D, whose L3 sequence is known (Bartlett and Joklik, 1988). The patterns of λ1 cleavage upon chymotrypsin treatment of T1L and T3D TC virions were found to be nearly identical (data not shown). The N terminus of λ1B was determined to have the sequence Ser-Val-Arg-Gly-Ala, corresponding to residues 345 to 349 in the deduced T3D λ1 sequence. Assuming that chymotrypsin does not also cleave sequences from the C terminus of λ1, the mass of λ1B is calculated to be 100 kDa, which is similar to its M_r = 96K determined from gradient gels (data not shown). These results indicate that the sequence removed from the cleaved λ1 molecules in TC subvirion particles represents an N-terminal region of the protein, with a sequence-defined mass of 37 kDa. It is noteworthy that the N-terminal region of λ1 is more hydrophilic than

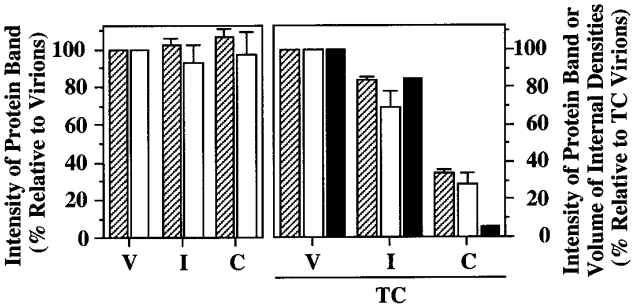

FIG. 6. Quantitation of λ1 and λ3 proteins compared with volumes of internal densities in TC particles. Intensities of the λ1 (hatched) and λ3 (white) protein bands from six types of orthoreovirus particles—virions, ISVPs, cores, and corresponding TC particles—were measured from SDS–polyacrylamide gels by phosphor imaging. Values are shown as a mean percentage relative to the amounts of these proteins in virions or TC virions. Error bars indicate standard deviations for four determinations each. The estimated volumes of internal densities in TC particles (black) at a density contour of −11 (see text and Table 1) are also shown as a percentage relative to the volume in TC virions.

the rest of the protein, has been implicated in the RNA-binding activity of λ1 (Lemay and Danis, 1994), contains a zinc-finger motif (Bartlett and Joklik, 1988), and contains other motifs characteristic of ATPases (Bartlett and Joklik, 1988) and RNA helicases (Noble and Nibert, 1997; Bisaillon *et al.,* 1997).

Reduced amounts of intact λ3 protein in TC ISVPs and TC cores

Previous studies with TC particles did not address the status of λ3, the orthoreovirus RNA polymerase (Drayna and Fields, 1982; Koonin, 1992; Starnes and Joklik, 1993), due to its low copy number, its comigration with λ2 in phosphate–urea–SDS gels, and a lack of protein-specific antisera (Smith *et al.,* 1969; White and Zweerink, 1976). Tris–glycine–SDS gels formed with reduced levels of bisacrylamide provide good separation of λ3 from λ1 and λ2 (Cleveland *et al.,* 1986), which we confirmed by Western blot analysis (Fig. 7A) using a polyclonal anti-λ3 serum (Cashdollar, 1994). We next used these gels to analyze λ3 in virions and TC virions of orthoreovirus T1L as well as in subvirion particles derived from each. Stained gels showed that the levels of intact λ3 were similar in virions, ISVPs, and cores but were decreased in TC ISVPs, and further decreased in TC cores, relative to TC virions (data not shown). Western blot analysis using the anti-λ3 serum gave similar results (Fig. 7B).

To quantify levels of λ3 protein in the different particles, we performed phosphor imaging as described for λ1 A representative gel (Fig. 7C) shows the decreased levels of λ3 in TC subvirion particles. For comparisons between lanes, the amount of λ3 was standardized to the σ2 band, which remained constant across all particles (see Figs. 5 and 7; Smith *et al.,* 1969; White and Zweerink, 1976). Results indicated that although the levels of intact λ3 in subvirion particles approached 100% of that in virions (93 ± 9% in ISVPs, 97 ± 12% in cores), its levels were reduced in TC subvirion particles relative to TC virions (69 ± 8% in TC ISVPs, 28 ± 6% in TC cores) (Fig. 6). Similar results were obtained with other plaque-derived clones of orthoreovirus T1L, again indicating that these are consistent properties of the T1L TC particles prepared by us.

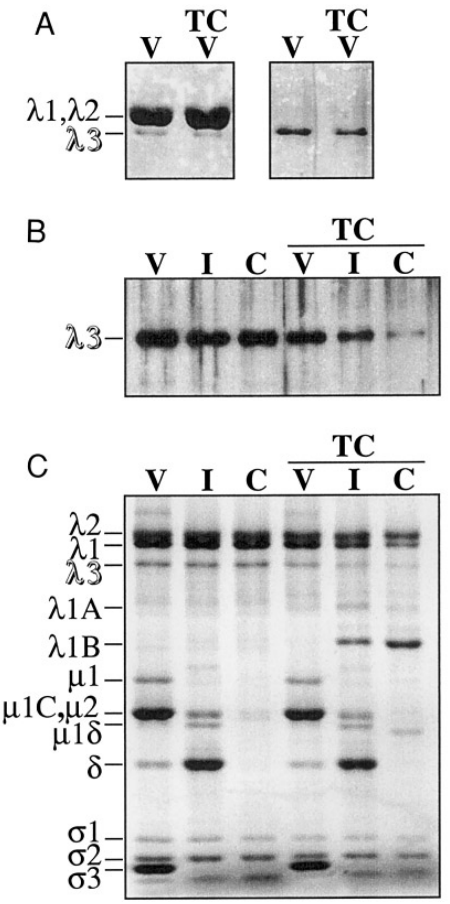

FIG. 7. Status of λ3 protein in virions, TC virions, and subvirion particles of each. Status of the λ3 protein in six types of orthoreovirus particles (see Fig. 5 legend for designations) was ascertained by SDS–PAGE and other methods. (A) To confirm the identity of the λ3 band, 6×10^{11} virions or TC virions were run in each gel lane, transferred to nitrocellulose, reversibly stained (left), and subjected to Western blotting with polyclonal anti-λ3 antibodies (Cashdollar, 1994) (right). The lanes were overloaded to obtain a dark λ3 signal, which caused the λ1 and λ2 bands to be distorted. (B) Samples containing 1×10^{11} viral particles were run in each gel lane, transferred to nylon, and either stained (data not shown) or probed with the polyclonal anti-λ3 antibodies. (C) Samples containing 6×10^{10} [^{35}S]methionine/cysteine-labeled viral particles were run in each gel lane and visualized by phosphor imaging. This gel was one used for the quantitations of λ3 shown in Fig. 6. The positions of orthoreovirus proteins are indicated in each panel. In (A) and (B), only the region of the blot surrounding the λ3 protein is shown.

Reduced amounts of intact μ2 protein in TC ISVPs and TC cores

As with λ3, previous studies with TC particles did not fully address the status of μ2, a putative cofactor for the polymerase (Yin *et al.,* 1996; Noble and Nibert, 1997), due to its low copy number, comigration with outer-capsid protein μ1C in virions and ISVPs, and lack of protein-specific antisera (Smith *et al.,* 1969; White and Zweerink, 1976). Since μ2 migrates close to the abundant μ1C protein in all gel systems we tested, we were unable to compare the amounts of μ2 in different particles by staining or phosphor imaging. We instead used Western blots to visualize μ2, employing a polyclonal anti-μ2 antiserum (Zou and Brown, 1995). Reduced-bis gels provided the best separation of μ2 from μ1C for these experiments. Using these methods, we showed that the levels of intact μ2 were similar in virions, ISVPs, and cores but were decreased in TC ISVPs, and further decreased in TC cores, relative to TC virions (Fig. 8). Although we have not quantified the levels of μ2 in different particles, the available data indicate that μ2 is cleaved in a similar qualitatively pattern to those of λ1 and λ3 in TC subvirion particles.

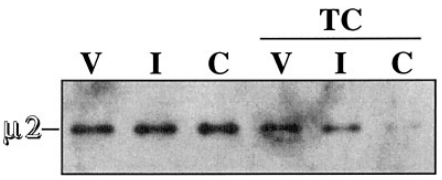

FIG. 8. Status of $\mu 2$ protein in virions, TC virions, and subvirion particles of each. Status of the $\mu 2$ protein in six types of orthoreovirus particles (see Fig. 5 legend for designations) was determined by SDS–PAGE and Western blotting. Samples containing 5×10^{10} viral particles were run in each gel lane. Only the region of the blot near the $\mu 2$ protein is shown.

Correlation between protein levels and volumes of internal densities in TC particles

For comparisons with data for proteins $\lambda 1$ and $\lambda 3$ above, we analyzed the electron-density maps to estimate the volumes of internal structures in the three types of TC particles. Densities between radii 246 Å (inner surface of the core shell) and 170 Å (beneath the flower-like structures) were included in the calculations. Volumes were calculated at a series of density contours (Table 1) before trying to define which contour best represents the true structures in each map. Since protein data suggest that $\lambda 3$, $\mu 2$, and an N-terminal portion of $\lambda 1$ form the internal structures in TC virions, we used current estimates for the sizes and copy numbers of those proteins or protein regions, and 1.30 g/cm^3 as an average protein density, to calculate that the internal structures should occupy a total volume of $\sim 9 \times 10^6$ Å^3. A contour of -11 (our units, $\sim$2.5 SD from external noise in the TC virion map) best approximated this figure, yielding a structure volume of 8.8×10^6 Å^3 between radii 246 and 170 Å. At this same density contour ($\sim$2.5 SD from external noise in the TC ISVP map and $\sim$3.9 SD from external noise in the TC core map), the volumes between 246 and 170 Å in TC ISVPs and TC cores were measured to be 7.4 and 0.5×10^6 Å^3, respectively. These values translate to relative values of 100, 84, and 6% for TC virions, TC ISVPs, and TC cores, respectively, which correlate with the quantitative data for $\lambda 1$ and $\lambda 3$ obtained by phosphor imaging as shown in Fig. 6. It is evident from Table 1 that the calculated volumes of internal structures are strongly dependent on the density contours at which the different maps are analyzed and compared; however, the trend of modestly reduced internal densities in TC ISVPs and more substantially reduced internal densities in TC cores is clear. There is also some methodological debate about whether properly scaled reconstructions, such as those for TC particles in this study, are more validly compared at the same density contour or at the same number of standard deviations from the mean noise of each map. We have used the former approach in this study, but the strength of correlations between protein levels and volumes of internal densities in TC particles is even greater using the latter approach (see Table 1, e.g., comparing the three TC particles at 2.7 SD from mean noise).

DISCUSSION

Model for how internal structures in TC particles can be cleaved by chymotrypsin

A question that arises from this study is how internal proteins in TC particles can be cleaved by chymotrypsin, since there are no evident holes through the inner

TABLE 1

Volumes of Internal Structures in TC Particles at Different Density Contours

Density contour[a]	TC virions			TC ISVPs			TC cores		
	SD[b]	Volume[c]	Volume %[d]	SD	Volume	Volume %	SD	Volume	Volume %
−7	1.8	14.2	100	1.9	13.8	97	2.7	2.1	15
−8	2.0	12.8	100	2.0	12.4	97	3.0	1.6	13
−9	2.2	11.3	100	2.2	9.7	86	3.3	0.9	8
−10	2.3	10.0	100	2.4	8.6	86	3.6	0.7	7
−11[e]	2.5	8.8	100	2.5	7.4	84	3.9	0.5	6
−12	2.7	7.7	100	2.7	5.5	71	4.2	0.3	4
−13	2.9	6.7	100	2.8	4.8	72	4.5	0.3	4
−14	3.0	6.0	100	3.0	4.2	70	4.8	0.2	3
−15	3.2	5.2	100	3.2	3.7	71	5.1	0.2	4

[a] Our arbitrary units.

[b] Number of standard deviations from noise that is represented by each density contour. Mean noise and standard deviation of noise were measured at a radius just beyond the outermost limit of each particle that each contour level.

[c] Volume of structures between radii 246 and 170 Å (lower limit of core shell and flower-like structures, respectively). Units = Å$^3 \times 10^{-6}$.

[d] Volume of structures between radii 246 and 170 Å, expressed as a percentage relative to the volume in TC virions at the same density contour.

[e] Density contour used for particle comparisons as described in text is highlighted by underlining.

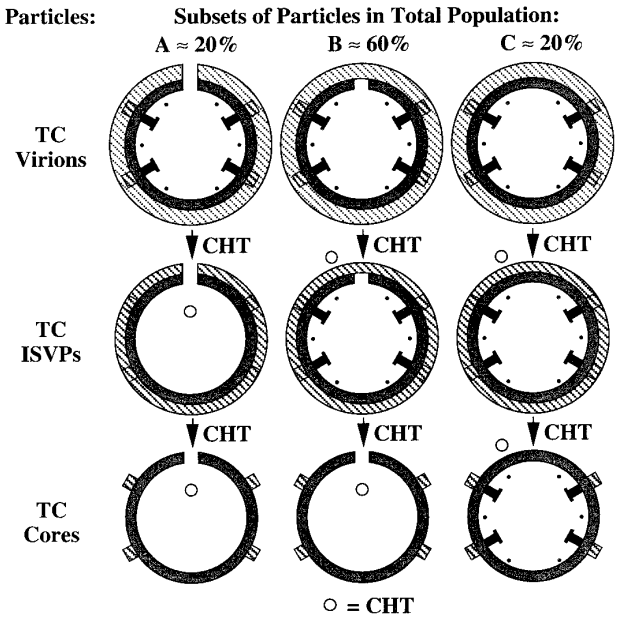

FIG. 9. Model explaining chymotrypsin cleavage of internal structures in TC particles and amounts of cleavage in TC ISVPs and TC cores. Three subpopulations of TC virions are hypothesized to exist at approximate proportions of 20% (A), 60% (B), and 20% (C) in the total population. Holes in both the inner (solid) and outer (hatched) capsids (in subpopulation A) or in the inner capsid only (in subpopulation B) allow chymotrypsin (CHT, open circle) to access the particle interior under different digestion conditions. In digestions yielding TC ISVPs, chymotrypsin can access the particle interior only in subpopulation A, reducing the average levels of internal densities and protein regions in all TC ISVPs by ~20%, to ~80% the levels in TC virions. In digestions yielding TC cores, chymotrypsin can access the particle interior in both subpopulations A and B, reducing the average levels of internal densities and protein regions in all TC cores by ~80%, to ~20% the levels in TC virions.

capsid that could permit entry of this >30-Å-diameter protein (see Fig. 2). One possibility might be that such holes are regularly opened as the capsid breathes in solution; however, the required size of holes makes this seem unlikely. In addition, the intermediate levels of cleavage seen in TC ISVPs and TC cores—reflected in both the densities of internal structures and the levels of intact λ1, λ3, and μ2 proteins—cannot be explained by the regular cleavage of proteins that are symmetrically arranged in an icosahedral lattice, as would be expected if chymotrypsin were gaining access to the interiors of all particles. For example, it is difficult to see why chymotrypsin should have cleaved only $0.3 \times 12 \approx 4$ of the λ3 molecules in each TC ISVP and only $0.7 \times 12 \approx 9$ of the λ3 molecules in each TC core. We think these observations are best explained if the original population of TC virions was heterogeneous, with the internal proteins in subpopulations exhibiting different susceptibilities to chymotrypsin cleavage due to the irregular presence of defects in the viral capsid(s). A model for how this might occur in agreement with our data is presented in Fig. 9.

Flower-like structures as complexes containing portions of proteins λ1, λ3, and μ2

One interpretation of evidence that internal densities and intact proteins λ1, λ3, and μ2 are reduced in concert in TC subvirion particles is that each of the flower-like structures comprises a complex of these proteins, including 10 copies of a 37-kDa N-terminal portion of λ1 (see below), a portion of one λ3 molecule per fivefold axis (see below), and most or all of the μ2 protein in particles. Another possibility, however, is that one or more of the protein regions lost from TC subvirion particles contribute not to the flower-like structures, but to less well ordered features inside these particles, which are also reduced by proteolysis (e.g., the disconnected densities near the threefold axes that are most prominent inside TC virions (Figs. 2B and 2C)). Immunoprecipitation data demonstrating pairwise interactions among all three λ proteins (Starnes and Joklik, 1993) are consistent with our interpretation that portions of both λ1 and λ3 are localized to sites near λ2 and the fivefold axes. In the case of μ2, however, no direct evidence for interactions with other viral proteins has yet been obtained.

Since the flower-like structures are found near the fivefold axes, there are two general possibilities for the nature of the real structures versus the structures as they appear in reconstructions. One is that the five petals represent a structural element that is indeed found in five copies around each fivefold axis. The other is that the petals represent an asymmetrically placed structure that is present in fewer than five copies (perhaps as few as one copy) per fivefold axis and is reproduced at the remaining sites by averaging during the reconstruction process. Given the limitations of current data, we cannot yet distinguish which of these possibilities is correct (but see discussion regarding λ1 below).

Copies of λ1 and its N-terminal Protease-sensitive Region

Data for λ1 in this study are interesting in light of recent findings with yeast L-A virus (Cheng *et al.,* 1994), bacteriophage φ6 (Butcher *et al.,* 1997), and rotavirus (Lawton *et al.,* 1997b). The RNA-juxtaposed capsids of these other double-stranded RNA viruses comprise 120 subunits arranged as asymmetric dimers in a $T = 1$ lattice. Since λ1 is also present in 120 copies per orthoreovirus particle (Smith *et al.,* 1969), it may be similarly arranged. Since an ~37-kDa, N-terminal region of λ1 (λ1N) contributes to the internal densities in orthoreovirus TC particles according to this study, then this region from the two λ1 molecules in each putative dimer may project into the particle at two different symmetry positions in the capsid (see Fig. 10). Thus, as one possible explanation, the five petals of each structure (Fig. 4) might represent the N termini from only one set of λ1 molecules, whereas the other set of λ1 N termini form other structures. Although the arrangement of the λ1 N

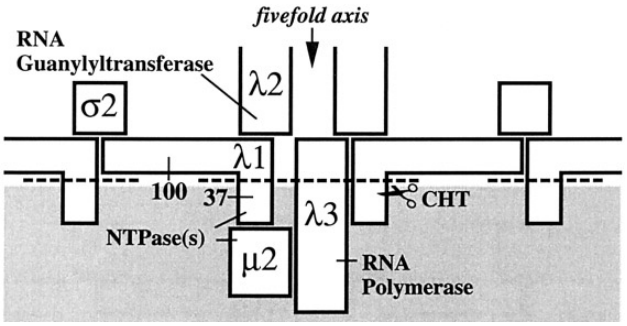

FIG. 10. Model for protein contributions to the internal densities in orthoreovirus TC particles. Sites of cleavage by chymotrypsin (CHT, scissors) to detach and degrade the internal proteins are indicated by dotted lines. The proposed locations of the C-terminal (100-kDa) and N-terminal (37-kDa) portions of λ1 are indicated. Relative positions of σ2 and C-terminal portions of λ1 in the protein shell remain unknown. The locations of λ3 and μ2 are also unknown except that λ3 can interact with both λ1 and λ2 in solution (Starnes and Joklik, 1993). Only the base of the λ2 protein is included in the diagram. The region occupied by dsRNA in genome-containing particles is indicated by shading. See text for additional explanations.

termini will be discerned more clearly only with higher resolution data, evidence that λ1 mediates an NTP-dependent enzymatic activity (Noble and Nibert, 1997; Bisaillon *et al.,* 1997) is consistent with our proposal that λ1 contributes to the putative transcriptase complexes, perhaps acting as an RNA helicase at some stage(s) of the transcription cycle (Noble and Nibert, 1997; Bisaillon *et al.,* 1997). It is notable that an N-terminal region of VP2, the λ1 analogue in rotaviruses, also projects into the particle interior (Lawton *et al.,* 1997b).

The moving-template model of transcription by orthoreovirus and other dsRNA viruses

By detecting the flower-like structures at the fivefold axes of TC particles and providing evidence that the RNA polymerase protein λ3 is one of its constituents, our results support the moving-template model of orthoreovirus transcription. This model states that complexes of the viral transcriptase enzymes are bound at specific sites in the inner capsid, necessitating movement of both product and template RNAs during transcription (Joklik, 1983; Shatkin and Kozak, 1983). While the molecular mechanisms of RNA translocation in orthoreovirus transcription are not understood, their study may provide insights into the spatial and mechanical aspects of transcription in other systems.

Recent 3-D reconstructions of rotavirus particles, another member of the family Reoviridae, revealed internal structures with similar morphology to those shown here for orthoreovirus (Prasad *et al.,* 1996). These structures were also found at the fivefold axes and appeared to be formed in part by the rotavirus RNA polymerase protein VP1. Other recent reconstructions of transcribing rotavirus particles indicated that the viral mRNAs exit the particle through one or more pores surrounding the fivefold axes (Lawton *et al.,* 1997a). Thus, the anchoring of transcriptase complexes at particle fivefold axes as part of a moving-template mechanism of transcription may be shared by viruses in this family.

Although grouped in a different virus family (Totiviridae), the L-A virus of yeast is another dsRNA virus that can be inferred to utilize a moving-template mechanism of transcription. The RNA polymerase of L-A is present in virus particles as a C-terminal extension of the gag capsid protein (gag-pol), formed by a ribosomal frameshift (Wickner, 1996). In this case, the covalent linkage between the polymerase and capsid proteins clearly necessitates the movement of template RNAs during transcription. It remains to be determined whether this strategy of transcription is common to all dsRNA viruses and whether it reflects evolutionary constraints associated with a dsRNA genome.

Juxtaposition of viral transcription and capping enzymes

The putative transcriptase complexes in TC particles are juxtaposed with pentamers of λ2, which mediates the RNA guanylyltransferase reaction (Cleveland *et al.,* 1986; Fausnaugh and Shatkin, 1990; Mao and Joklik, 1991) and may mediate one or both of the RNA methyltransferase reactions (Seliger *et al.,* 1987; Koonin, 1993) in mRNA capping. The proximity of these components suggests that the transcription and capping enzymes are arranged for efficient transfer of the 5′ end of nascent mRNAs between them (see Fig. 10). The protein that mediates the first step in capping—the RNA triphosphatase that cleaves the γ phosphate from the 5′ end of each mRNA—has not been definitively assigned in orthoreoviruses. However, because this enzyme acts on the product of the polymerase to generate the substrate for the guanylyltransferase, it seems likely to be localized within or near each flower-like structure as well. An NTPase activity associated with λ1 (Noble and Nibert, 1997; Bisaillon *et al.,* 1997; Bisaillon and Leymay, 1997) and/or μ2 (Noble and Nibert, 1997) may represent this enzyme. Juxtaposition of the transcription and capping enzymes is also found in rotavirus particles (Prasad *et al.,* 1996). Since direct interactions between RNA polymerases and RNA processing enzymes have been shown for other, non-dsRNA, viruses, including vaccinia virus (Shuman *et al.,* 1987), brome mosaic virus (Smirnyagina *et al.,* 1996), and Sindbis virus (Lemm *et al.,* 1994), the more unique aspect with members of the Reoviridae is that the enzymes for transcription and capping are directly associated with the viral icosahedral capsid(s).

MATERIALS AND METHODS

Preparation of viral particles

Virions and TC virions of orthoreovirus T1L or T3D were purified as described (Furlong *et al.,* 1988). To obtain [^{35}S]methionine/cysteine-labeled particles, 5 mCi of Tran^{35}S-label (ICN Biochemicals) was added per 4×10^8 cells in spinner culture. Freon-extracted lysates of infected cells were layered atop 1.25 to 1.45 g/cm^3 CsCl gradients and spun at 23,000 rpm for ≥2 h in an SW28.1 rotor (Beckman). Bands containing virions ($\rho \approx 1.36$ g/cm^3) and TC virions ($\rho \approx 1.30$ g/cm^3) were collected separately and dialyzed in virion buffer (Furlong *et al.,* 1988). To purify and concentrate the particles further, they were run on a 1.20 to 1.40 g/cm^3 CsCl gradient at 35,000 rpm for ≥2 h in an SW50.1 rotor (Beckman) and treated as above. Virion concentrations were determined from the relationship 1.0 $A_{260} = 2.1 \times 10^{12}$ virions/ml (Smith *et al.,* 1969). TC virion concentrations were determined from the empirically determined relationship 1.0 $A_{280} = 6.6 \times 10^{12}$ TC virions/ml.

ISVPs or TC ISVPs of orthoreovirus T1L were prepared by digesting virions or TC virions at a concentration of 1×10^{13} particles/ml with 200 μg/ml α-chymotrypsin (Sigma) for 20–30 min at 37°C in virion buffer. Cores or TC cores of orthoreovirus T1L were prepared by digesting either virions or TC virions at a concentration of 6×10^{13} particles/ml with 200 μg/ml α-chymotrypsin for 1.5–3 h at 37°C in virion buffer. TC cores of orthoreovirus T3D were prepared by digesting TC virions at a concentration of 2×10^{13} particles/ml with 200 μg/ml α-chymotrypsin for 1.5 h at 37°C in virion buffer. Digestions were terminated by adding phenylmethylsulfonyl fluoride to 1 to 5 mM and chilling on ice. To purify TC ISVPs and TC cores, digests were run on a 1.20 to 1.40 g/cm^3 CsCl gradient at 35,000 rpm for ≥2 h in an SW50.1 rotor (Beckman), after which the TC ISVPs and TC cores were dialyzed in virion buffer and core buffer (Coombs *et al.,* 1990), respectively. Flocculated material that sometimes cobanded with TC cores was removed from dialyzed samples by brief microcentrifugation.

Cryo-TEM, image processing, and 3-D reconstructions

Cryo-TEM was performed as described (Baker *et al.,* 1988; Dryden *et al.,* 1993). Samples were vitrified by adhering a 4-μl droplet of sample to a hydrophilic holey-carbon grid, blotting the droplet, and plunging the grid into liquid ethane. Grids were stored in liquid nitrogen before transfer to a cooled Gatan cryospecimen holder, which was maintained at ~−170°C in the microscope. Micrographs were recorded in a Philips EM420 electron microscope at a nominal magnification of 30,000×, with the objective lens at ~1 μm underfocus. Specimens were irradiated under low-dose codnitions, ~8 electrons/ Å^2. TC virions and TC ISVPs adopted preferential orientations in the vitrified samples with a fivefold axis normal to the plane of the grid. The two particles were mixed to minimize systematic errors during microscopy (Yeager *et al.,* 1994), and images were recorded with grids tilted by 15° or 25° relative to the electron beam to generate a diverse set of particle orientations (Dryden *et al.,* 1993).

Micrographs selected for processing displayed minimal specimen drift and image astigmatism and contained a large number of well-separated particles. Micrographs were digitized on a rotating-drum densitometer (Optronics) at 25-μm intervals, corresponding to an effective step size in the specimen of ~8.3 Å per pixel. Particles appropriate for processing were selected, stored, and scaled as previously described (Baker *et al.,* 1988; Dryden *et al.,* 1993). Magnifications were determined by scaling equivalent density peaks in circularly averaged images of different particles to the same radius (Belnap *et al.,* 1993). This gave calibrated values of 29,600× and 31,200×, respectively, for the 15°- and 25°-tilted views of mixed TC virions and TC ISVPs and 30,500× for the untilted views of TC cores.

Polar Fourier transform and Fourier–Bessel routines were used to compute 3-D reconstructions from selected images (Baker and Cheng, 1996; Fuller *et al.,* 1996). Reconstructions of virions, ISVPs, and cores (Dryden *et al.,* 1993) from which inner densities were removed to mimic TC particles were used as initial models. Radial density plots were used to adjust the scale of models to the TC particle data (Olson and Baker, 1989; Belnap *et al.,* 1993). An initial search for particle orientations was done at 1° intervals, with Fourier-transformed data filtered to remove high (>1/40 Å^{-1}) and low (<1/250 Å^{-1}) spatial frequencies. This led to identification of ~20 particle images for each that were used to compute initial 3-D models at 35-Å resolution (Baker and Cheng, 1996; Fuller *et al.,* 1996). After several cycles of refinement, in which the resolution limit was gradually increased, all acceptable particles were included and no more improvement was obtained in the correlation coefficients between images and reprojections of the density maps in corresponding view directions (Dryden *et al.,* 1993). For each reconstruction, the distribution of particle orientations was relatively uniform within the asymmetric unit. In each reconstruction the inverse eigenvalue spectrum for all spatial frequencies (<1/30 Å) was less than 1, confirming that no sampling errors were generated during Fourier inversion (Crowther, 1971).

To assess its quality, each data set was divided in two, each of which was refined independently (Baker *et al.,* 1991). TC virion and TC ISVP images recorded at different tilt angles were also analyzed independently. Such analyses also permitted the resolution of each data set to be assessed. No visual differences between the independent reconstructions for each particle type were noted, and correlation coefficients between reconstructed den-

sity maps and respective images were greater than 0.5 at 30-Å resolution. Final reconstructions were computed from 75, 87, and 114 particles for TC virions, TC ISVPs, and TC cores, respectively. Reconstructions of both TC particles and the respective genome-containing particles (Dryden *et al.,* 1993) were calculated to the same resolution limit (30 Å) and scaled to the same size (Belnap *et al.,* 1993), contrast, and average density to permit valid comparisons. The reconstructions of TC subvirion particles were scaled to the TC virion by refining size, contrast, and density values to maximize the correlation coefficients for densities between radii 246 and 318 Å.

Protein electrophoresis and quantitation

Samples were disrupted by boiling in sample buffer for 2 min. Continuous phosphate–urea–SDS gels were run at 50 V for 16 h. Discontinuous Tris–glycine–SDS gels were run at 20 mA for ~15 h through the 4% stacking gel (2.6% bisacrylamide) and then at 50 mA for ~2.5 h through the 4–9% resolving gel (1.3% bisacrylamide). Both gel types were cast to be 15 mm thick, 16 cm long, and 20 cm wide. Gels of [^{35}S]methionine/cysteine-labeled viral proteins were dried onto filter paper under vacuum and exposed to phosphor imager screens (Molecular Dynamics) for at least 48 h. ImageQuant software (Molecular Dynamics) was used for quantitating protein bands. The intensity of each band was corrected for background by subtracting the intensity of a corresponding area of a blank lane on the same gel. The amount of a particular protein in each particle type was expressed as a fraction of another protein (λ2 or σ2) which, according to absolute intensities, remained unchanged between particle types. Changes in protein levels between particle types were determined by expressing the above ratio as a percentage of the ratio of the corresponding virion (full or TC) run on the same gel.

Western blotting and N-terminal Sequencing

Proteins were transferred from 4–9% reduced-bis gradient gels. Alkaline phosphatase-conjugated goat α-rabbit antibodies (Bio-Rad) were used as secondary antibody. To confirm the λ3 band on reduced-bis gels, 6×10^{11} particles were run per lane. Proteins were transferred to nitrocellulose membrane (Bio-Rad), stained with a reversible detection kit (Sigma), probed with polyclonal α-λ3 antibodies (Cashdollar, 1994), and detected by a BCIP/NBT colorimetric assay (Bio-Rad). For detection of λ3 or μ2 in different particles, 1×10^{11} (for λ3) or 5×10^{10} (for μ2) particles were run per lane. The proteins were transferred to Immun-Lite nylon membrane (Bio-Rad), probed with either α-λ3 antibodies or a polyclonal α-μ2 serum (Zou and Brown, 1995), and detected by chemiluminescent assay (Bio-Rad).

N-terminal sequencing was performed as described (Nibert and Fields, 1992). A total of 2.5×10^{12} purified TC cores of orthoreovirus T3D were disrupted at 60°C and loaded in two lanes atop a 6% gel. Following electrophoresis, proteins were electroblotted to polyvinylidene fluoride membrane (Applied Biosystems). Proteins on the membrane were stained with Ponceau S, and λ1B was excised for N-terminal sequencing at the Harvard University Microchemistry Laboratory (Cambridge, MA). Results were reported with confidence from 29 to 51 pmol of amino acid detected per cycle.

Note added in proof. A recent study provides evidence that the μ2 protein is present in about 20 copies perorthoreovirus particle, possibly two copies per fivefold axis or genome segment (K.M. Coombs (1998) *Virology* 243, 218–228). This contrasts with previous estimates of 12 and suggests that the μ2 structure shown in Fig. 10 may represent a dimer of that protein.

ACKNOWLEDGMENTS

We are grateful to L. W. Cashdollar (Medical College of Wisconsin) and E. G. Brown (University of Ottawa) for providing antibodies; W. S. Lane and colleagues (Harvard Microchemistry Lab) for N-terminal sequencing; E. C. Freimont and R. L. Margraf for technical support; and S. C. Harrison, C. Luongo, S. Noble, and L. A. Schiff for helpful comments on the manuscript. This work was supported by NIH Grants AI13178 (B.N.F.), GM33050 (T.S.B.), and AI39533 (M.L.N.) and a grant from the Lucille P. Markey Charitable Trust to the Institute for Molecular Virology (University of Wisconsin-Madison). Additional support to D.L.F. was provided by NIH Grant GM08349 to the Biotechnology Training Program, University of Wisconsin-Madison; to B.N.F. by the Shipley Institute of Medicine; and to M.L.N. by a Shaw Scientist Award from the Milwaukee Foundation (Milwaukee, WI).

REFERENCES

Baker, T. S., and Cheng, R. H. (1996). A model-based approach for determining orientations of biological macromolecules imaged by cryoelectron microscopy. *J. Struct. Biol.* 116, 120–130.

Baker, T. S., Drak, J., and Bina, M. (1988). Reconstruction of the three-dimensional structure of simian virus 40 and visualization of the chromatin core. *Proc. Natl. Acad. Sci. USA* 85, 422–426.

Baker, T. S., Newcomb, W. W., Olson, N. H., Cowsert, L. M., Olson, C., and Brown, J. C. (1991). Structures of bovine and human papilloma viruses: Analysis by cryoelectron microscopy and three-dimensional image reconstruction. *Biophys. J.* 60, 1445–1456.

Banerjee, A. K., and Shatkin, A. J. (1970). Transcription in vitro by reovirus-associated ribonucleic acid-dependent polymerase. *J. Virol.* 6, 1–11.

Bartlett, J. A., and Joklik, W. K. (1988). The sequence of the reovirus serotype 3 L3 genome segment which encodes the major core protein λ1. *Virology* 167, 313–317.

Bartlett, N. M., Gillies, S. C., Bullivant, S., and Bellamy, A. R. (1974). Electron microscopy study of reovirus reaction cores. *J. Virol.* 14, 315–326.

Belnap, D. M., Grochulski, W. D., Olson, N. H., and Baker, T. S. (1993). Use of radial density plots to calibrate image magnification for frozen-hydrated specimens. *Ultramicroscopy* 48, 347–358.

Bisaillon, M., Bergeron, J., and Lemay, G. (1997). Characterization of the nucleoside triphosphate phosphohydrolase and helicase activities of reovirus λ1 protein. *J. Biol. Chem.* 272, 18298–18303.

Bisaillon, M., and Lemay, G. (1997). Characterization of the reovirus λ1 protein RNA 5′ triphosphatase activity. *J. Biol. Chem.* 272, 29954–29957.

Butcher, S. J., Dokland, T., Ojala, P. M., Bamford, D. H., and Fuller, S. D.

(1997). Intermediates in the assembly pathway of the double-stranded RNA virus phi6. *EMBO J.* 16, 4477–4487.

Cashdollar, L. W. (1994). Characterization and structural localization of the reovirus λ3 protein. *Res. Virol.* 145, 277–285.

Cheng, R. H., Caston, J. R., Wang, G.-J., Gu, F., Smith, T. J., Baker, T. S., Bozarth, R. F., Trus, B. L., Cheng, N., Wickner, R. B., and Steven, A. C. (1994). Fungal virus capsids, cytoplasmic compartments for the replication of double-stranded RNA, formed as icosahedral shells of asymmetric Gag dimers. *J. Mol. Biol.* 244, 255–258.

Cleveland, D. R., Zarbl, H., and Millward, S. (1986). Reovirus guanylyltransferase is L2 gene product λ2. *J. Virol.* 60, 307–311.

Coombs, K. M. (1996). Identification and characterization of a double-stranded RNA− reovirus temperature-sensitive mutant defective in minor core protein μ2. *J. Virol.* 70, 4237–4245.

Coombs, K. M., Fields, B. N., and Harrison, S. C. (1990). Crystallization of the reovirus type 3 Dearing core. Crystal packing is determined by the λ2 protein. *J. Mol. Biol.* 215, 1–5.

Crowther, R. A. (1971). Procedures for three-dimensional reconstruction of spherical viruses by Fourier synthesis from electron micrographs. *Philos. Trans. R. Soc. London Ser. B Biol. Sci.* 261, 221–230.

Drayna, D., and Fields, B. N. (1982). Activation and characterization of the reovirus transcriptase: Genetic analysis. *J. Virol.* 41, 110–118.

Dryden, K. A., Wang, G., Baker, T. S., Yeager, M. A., Nibert, M. L., Coombs, K. M., Furlong, D. B., and Fields, B. N. (1993). Early steps in reovirus infection are associated with dramatic changes in supramolecular structure and protein conformation: analysis of virions and subvirion particles by cryoelectron microscopy and image reconstruction. *J. Cell Biol.* 122, 1023–1041.

Fausnaugh, J., and Shatkin, A. J. (1990). Active site localization in a viral mRNA capping enzyme. *J. Biol. Chem.* 265, 7669–7672.

Fuller, S. D., Butcher, S. J., Cheng, R. H., and Baker, T. S. (1996). Three-dimensional reconstruction of icosahedral particles—The uncommon line. *J. Struct. Biol.* 116, 45–55.

Furlong, D. B., Nibert, M. L., and Fields, B. N. (1988). Sigma 1 protein of mammalian reoviruses extends from the surfaces of viral particles. *J. Virol.* 62, 246–256.

Furuichi, Y., Morgan, M., Muthukrishnan, S., and Shatkin, A. J. (1975). Reovirus messenger RNA contains a methylated, blocked 5′-terminal structure: ^{m7}G(5′)ppp(5′)G^{m}pCp-. *Proc. Natl. Acad. Sci. USA* 72, 362–366.

Haller, B. L., Barkon, M. L., Vogler, G. P., and Virgin, H. W., IV. (1995). Genetic mapping of reovirus virulence and organ tropism in severe combined immunodeficient mice: Organ-specific virulence genes. *J. Virol.* 69, 357–364.

Harvey, J. D., Bellamy, A. R., Earnshaw, W. C., and Schutt, C. (1981). Biophysical studies of reovirus type 3. IV. Low-angle x-ray diffraction studies. *Virology* 112, 240–249.

Joklik, W. K. (1983). The reovirus particle. *In* "The Reoviridae" (W. K. Joklik, Ed.), pp. 9–78. Plenum, New York.

Koonin, E. V. (1992). Evolution of double-stranded RNA viruses: A case for polyphyletic origin from different groups of positive-stranded RNA viruses. *Semin. Virol.* 3, 327–340.

Koonin, E. V. (1993). Computer-assisted identification of a putative methyltransferase domain in NS5 protein of flaviviruses and lambda 2 protein of reovirus. *J. Gen. Virol.* 74, 733–740.

Lawton, J. A., Estes, M. K., and Prasad, B. V. V. (1997a). Three-dimensional visualization of mRNA release from actively transcribing rotavirus particles. *Nature Struct. Biol.* 4, 118–121.

Lawton, J. A., Zeng, C.Q.-Y., Mukherjee, S. K., Cohen, J., Estes, M. K., and Prasad, B. V. V. (1997b). Three-dimensional structural analysis of recombinant rotavirus-like particles with intact and amino-terminal-deleted VP2: Implications for the architecture of the VP2 capsid layer. *J. Virol.* 71, 7353–7360.

Lemay, G., and Danis, C. (1994). Reovirus lambda 1 protein: Affinity for double-stranded nucleic acids by a small amino-terminal region of the protein independent from the zinc finger motif. *J. Gen. Virol.* 75, 3261–3266.

Lemm, J. A., Rumenapf, T., Strauss, E. G., Strauss, J. H., and Rice, C. M. (1994). Polypeptide requirements for assembly of functional Sindbis virus replications complexes: A model for the temporal regulation of minus- and plus-strand RNA synthesis. *EMBO J.* 13, 2925–2934.

Levin, D. H., Mendelsohn, N., Schonberg, M., Klett, H., Silverstein, S., Kapuler, A. M., and Acs, G. (1970). Properties of RNA transcriptase in reovirus subvirion particles. *Proc. Natl. Acad. Sci. USA* 66, 890–897.

Lucia-Jandris, P., Hooper, J. W., and Fields, B. N. (1993). Reovirus M2 gene is associated with chromium release from mouse L cells. *J. Virol.* 67, 5339–5345.

Mao, Z. X., and Joklik, W. K. (1991). Isolation and enzymatic characterization of protein λ2, the reovirus guanylyltransferase. *Virology* 185, 377–386.

Metcalf, P., Cyrklaff, M., and Adrian, M. (1991). The three-dimensional structure of reovirus obtained by cryo-electron microscopy. *EMBO J.* 10, 3129–3136.

Morgan, E. M., and Kingsbury, D. W. (1981). Reovirus enzymes that modify messenger RNA are inhibited by perturbation of the lambda proteins. *Virology* 113, 565–572.

Nibert, M. L., and Fields, B. N. (1992). A carboxy-terminal fragment of protein μ1/μ1C is present in infectious subvirion particles of mammalian reoviruses and is proposed to have a role in penetration. *J. Virol.* 66, 6408–6418.

Nibert, M. L., Schiff, L. A., and Fields, B. N. (1991). Mammalian reoviruses contain a myristoylated structural protein. *J. Virol.* 65, 1960–1967.

Noble, S., and Nibert, M. L. (1997). Characterization of an ATPase activity in reovirus cores and its genetic association with core-shell protein λ1. *J. Virol.* 71, 1282–1291.

Noble, S., and Nibert, M. L. (1997). Core protein μ2 is a second determinant of NTPase activities by reovirus cores. *J. Virol.* 71, 7728–7735.

Olson, N., and Baker, T. S. (1989). Magnification calibration and the determination of spherical virus diameters using cryoelectron microscopy. *Ultramicroscopy* 30, 281–298.

Powell, K. F., Harvey, J. D., and Bellamy, A. R. (1984). Reovirus RNA transcriptase: Evidence for a conformational change during activation of the core particle. *Virology* 137, 1–8.

Prasad, B. V. V., Rothnagel, R., Zeng, C. Q., Jakana, J., Lawton, J. A., Chiu, W., and Estes, M. K. (1996). Visualization of ordered genomic RNA and localization of transcriptional complexes in rotavirus. *Nature* 382, 471–473.

Rankin, J. T., Jr., Eppes, S. B., Antczak, J. B., and Joklik, W. K. (1989). Studies on the mechanism of the antiviral activity of ribavirin against reovirus. *Virology* 168, 147–158.

Seliger, L. S., Zheng, K., and Shatkin, A. J. (1987). Complete nucleotide sequence of reovirus L2 gene and deduced amino acid sequence of viral mRNA guanylyltransferase. *J. Biol. Chem.* 262, 16289–16293.

Shatkin, A. J. (1974). Methylated messenger RNA synthesis in vitro by purified reovirus. *Proc. Natl. Acad. Sci. USA* 71, 3204–3207.

Shatkin, A. J., and Kozak, M. (1983). Biochemical aspects of reovirus transcription and translation. *In* "The Reoviridae" (W. K. Joklik, Ed.), pp. 79–106. Plenum, New York.

Sherry, B., and Blum, M. A. (1994). Multiple viral core proteins are determinants of reovirus-induced acute myocarditis. *J. Virol.* 68, 8461–8465.

Shuman, S., Broyles, S. S., and Moss, B. (1987). Purification and characterization of a transcription termination factor from vaccinia virions. *J. Biol. Chem.* 262, 12372–12380.

Skehel, J. J., and Joklik, W. K. (1969). Studies on the in vitro transcription of reovirus RNA catalyzed by reovirus cores. *Virology* 39, 822–831.

Smirnyagina, E., Lin, N.-S., and Ahlquist, P. (1996). The polymerase-like core of brome mosaic virus 2a protein, lacking a region interacting with viral 1a protein in vitro, maintains activity and 1a selectivity in RNA replication. *J. Virol.* 70, 4729–4736.

Smith, R. E., Zweerink, H. J., and Joklik, W. K. (1969). Polypeptide

components of virions, top component and cores of reovirus type 3. *Virology* 39, 791–810.

Spencer, S. M., Sgro, J.-Y., Dryden, K. A., Baker, T. S., and Nibert, M. L. (1997). IRIS Explorer software for radial-depth cueing reovirus particles and other macromolecular structures determined by cryoelectron microscopy and image reconstruction. *J. Struct. Biol.* 120, 11–21.

Starnes, M. C., and Joklik, W. K. (1993). Reovirus protein λ3 is a poly(C)-dependent poly(G) polymerase. *Virology* 193, 356–366.

White, C. K., and Zweerink, H. J. (1976). Studies on the structure of reovirus cores: Selective removal of polypeptide λ2. *Virology* 70, 171–180.

Wickner, R. B. (1996). Viruses of yeast, fungi and parasitic microorganisms. *In* "Fields Virology" (B. N. Fields, D. M. Knipe, and P. M. Howley, Eds.), 3rd ed., pp. 557–585. Lippincott–Raven, Philadelphia.

Xu, P., Miller, S. E., and Joklik, W. K. (1993). Generation of reovirus core-like particles in cells infected with vaccinia viruses that express genome segments L1, L2, L3, and S2. *Virology* 197, 726–731.

Yeager, M., Berriman, J. A., Baker, T. S., and Bellamy, A. R. (1994). Three dimensional structure of the rotavirus haemagglutinin VP4 by cryoelectron microscopy and difference map analysis. *EMBO J.* 13, 1011–1018.

Yeager, M., Weiner, S., and Coombs, K. M. (1996). Transcriptionally active reovirus core particles visualized by electron cryo-microscopy and image reconstruction. *Biophys. J.* 70, A116.

Yin, P., Cheang, M., and Coombs, K. M. (1996). The M1 gene is associated with differences in the temperature optimum of the transcriptase activity in reovirus core particles. *J. Virol.* 70, 1223–1227.

Zou, S., and Brown, E. G. (1995). Stable expression of the reovirus μ2 protein in mouse L cells complements the growth of a reovirus ts mutant with a defect in its M1 gene. *Virology* 217, 42–48.